Investigating a Second Harmonic Radio Frequency Cavity for the Fermilab Booster

Maggie Lankford

The College of Wooster, Wooster OH 44691 USA

Fermilab Accelerator Division, Batavia, IL 60510 USA

(Dated: August 6, 2015)

Abstract

This is a study of building a second harmonic, perpendicularly tuned radio frequency cavity for the Fermilab Booster. Adding a second harmonic radio frequency cavity to the Booster accelerator will increase the beam intensity, allowing for more neutrino production and more precise measurements, the primary focus of Fermilab's experiments. A perpendicular biased tuner has less power loss than a parallel biased tuner and allows for a larger cavity voltage using the current power amplifier. This is primarily a comparison study of the real and model cavities to be built.

I. INTRODUCTION

In our quest to understand fundamental structure of the universe, we have discovered the existence of the neutrino which is now the primary focus at Fermi National Accelerator Lab (FNAL). To unravel the secrets of this elusive particle, improvements must be made to the accelerator complex, one of which involves the injection of beam from the linear accelerator (LINAC) to the Booster accelerator.

Adding a second harmonic radio frequency (RF) cavity in the Booster will increase the RF bucket area which can reduce space charge effects within the beam, given the beam consists of particles of the same charge. Overall, the effect of the second harmonic cavity is to increase the beam capture from the LINAC, leading to higher beam intensities and allowing for more neutrino production [2].

Due to the high quality factor of such a cavity and the limited space in the Booster tunnel, the group has chosen to build a cavity which is tuned by a perpendicular bias. To design a cavity using this non-traditional method of tuning, a model and many simulations are necessary to ensure success. The goals of this summer project are to simulate both the model and the real cavity using Poisson Superfish [1], and to build a physical model of the cavity to test its properties and troubleshoot. The combination of these two parts will give insight into the necessary design and the properties of the Booster cavity.

II. RADIO FREQUENCY CAVITY BASICS

The real RF cavity will be put into the Fermilab Booster, a synchrotron accelerator. It will consist of a coper coaxial line under vacuum with the inner and outer conductor shorted at one end as in Fig. 1. The beam line runs down the center of the inner conductor and so is shielded from the transverse magnetic field and the radial electric field until it reaches a gap. The length of the center conductor should be one quarter wavelength (of the radio frequency) so that the electric field is at a maximum at the point of the gap. The protons in the beam line will then see a maximum voltage across the gap.

Since the Booster is a synchrotron accelerator, the protons will travel the same path many times at different energy and speed. Consequently, the cavity must change in order for the beam to be continually in phase with the RF.

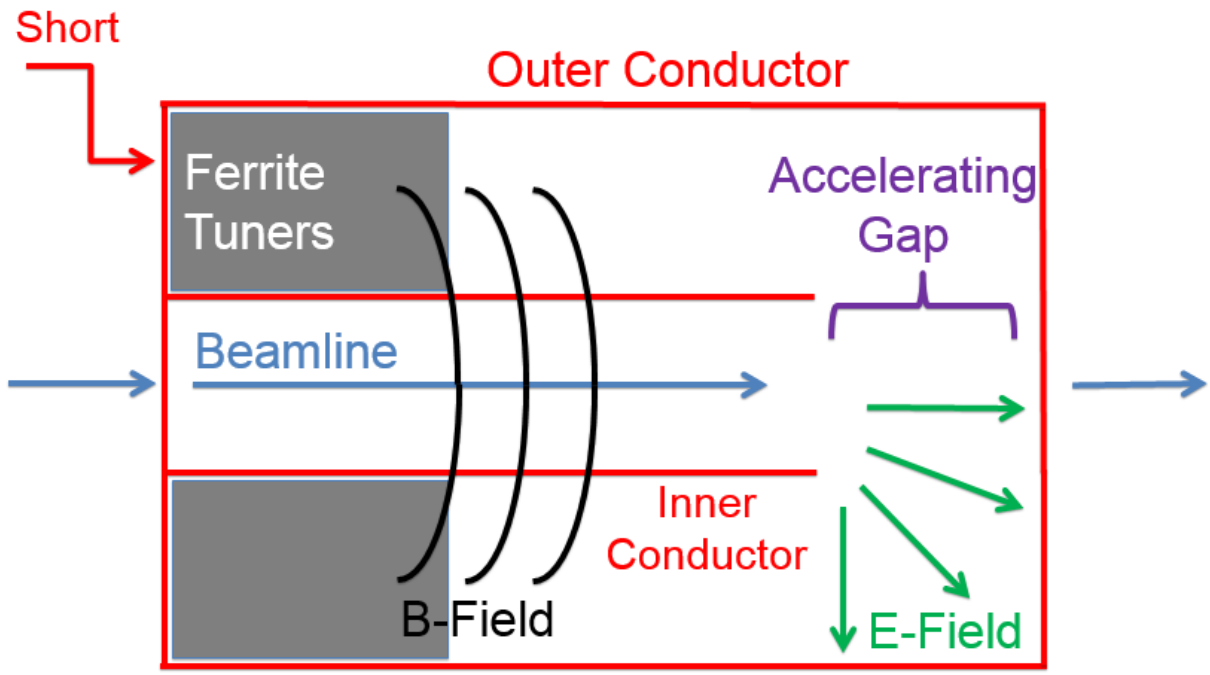

FIG. 1: A cross-sectional diagram of the RF cavity with the major components labeled.

At resonance, a standing wave exists in the cavity, and

$$v = \frac{c}{\sqrt{\mu\epsilon}} = f\lambda, \tag{1}$$

where v is the speed of light in a given medium, c is the speed of light in a vacuum, μ is permeability, ϵ is permittivity, f is frequency, and λ is the wavelength in a medium. Since the cavity is resonant at a quarter wavelength and the permittivity is fixed, a reasonable way to change the resonant frequency of the cavity is to change its permeability.

Ferrite material has the convenient property of a variable permeability which can be manipulated by changing the strength of magnetic field surrounding the material. By filling a region of the cavity with ferrite and putting it into a solenoid coil, the permeability of the ferrite and consequently the cavity can be changed.

The permeability of the ferrite is best described as a complex quantity

$$\mu = \mu' - i\mu'' \tag{2}$$

where μ'' describes the amount of loss and μ' is the tuning parameter, equivalent to the μ in Eq. 1. Both of these values are dependent on the bias magnetic field, and to characterize

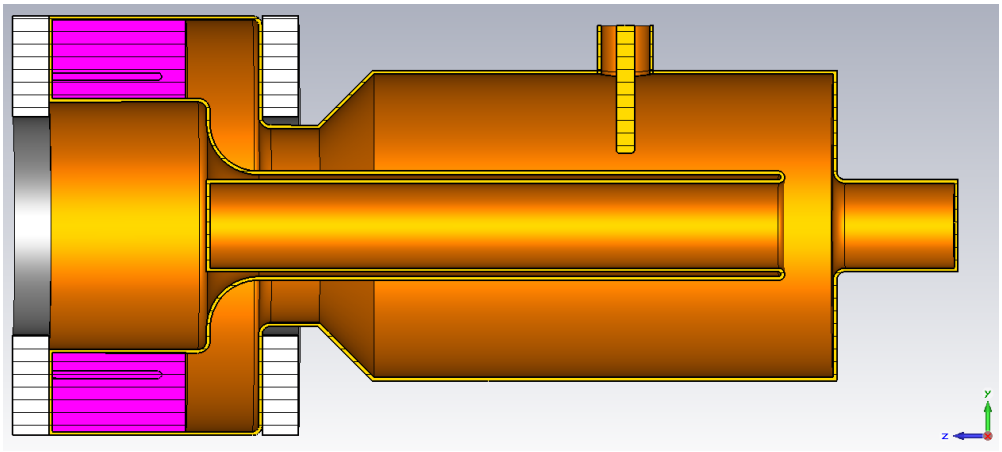

FIG. 2: Real cavity design cross-section in CST Microwave Studio simulation. The beam propagates from the left to the right. The garnet region is shown in purple at the left and the accelerating gap at the right.

the tuning and losses in the cavity we generally want to find their relationship.

This cavity is perpendicular biased tuned, meaning the induced magnetic field in the ferrite is perpendicular to the RF field. This method for biasing is less lossy than using a parallel bias, which has been used in most accelerators. A low loss means that the gap voltage is can be very large for a given input power. The perpendicular biasing of the cavity is also a space-saver in the tunnel because the high gap voltage allows us to use one cavity instead of two.

A cross-section of the real cavity design to date is shown in Fig. 2, and a model shown in Fig. 3. The model will not be under vacuum and has a scaled down ferrite garnet section due to solenoid size limits. Some dimensions of the model had to be changed for various reasons, the effects of which are addressed further in the simulations sections.

Overall, the model cavity will be used primarily to test the shunt impedance and the quality factor of the cavity. Shunt impedance is defined as

$$R_{sh} = \frac{V_{peak}^2}{2P}, \tag{3}$$

where V_{peak} is the peak voltage in the gap and P is the power dissipation. The quality factor is defined as

$$Q = \omega \frac{U}{P}, \tag{4}$$

where ω is the angular frequency and U is the stored energy.

These two factors together are used to characterize the cavities, how they compare, and how they change over the given frequency range.

III. MODEL CAVITY SIMULATIONS

A. Structural Changes

An ideal model cavity was designed as a scaled down version of the real Booster cavity, however, small changes were implemented which save in cost and make assembly easier. These changes include decreasing the outer diameter of the inner conductor in the air section, decreasing the inner diameter of the outer conductor in the air section, and increasing the outer diameter of the inner conductor in the garnet section. The final blueprints of the model cavity are shown in Fig 3. The change in the model cavity from each modification was studied using Poisson Superfish, but most importantly, the differences between the real cavity and the final model cavity were studied.

The software Poisson Superfish was designed by Los Alamos National Laboratory for the specific purpose of simulating RF cavities. In this program, the RF volume is stated with cylindrical symmetry about the beam axis. The properties of the garnet region are also specified, including the complex permittivity and permeability. Since the cavity is tuned by changing the permeability, in this study the appropriate permeability was chosen so that the fundamental frequency of the model cavity was 76 MHz. A frequency scan is initially performed from 0 to 1 GHz to ascertain the approximate frequencies of the higher order modes (HOM) in that range, and then an individual run gives the quality factor and the shunt impedance at each resonant frequency. An inspection of the electric field arrows in the RF volume confirms the resonant transverse electromagnetic (TEM) mode of the cavity. Resonant modes of transverse magnetic (TM) or transverse electric (TE) waves occur in the real cavity but are not included in the study.

A Poisson Superfish analysis of the ideal model cavity was then performed, followed by an analysis with the three structural modifications. Modification one decreased the outer diameter of the inner conductor in the air section from nominal 3.543 inches to 3.50 inches because pipe is readily available in this size. Modification two decreased the inner diameter of the outer conductor in the air section from nominal 9.843 inches to 9.832 inches

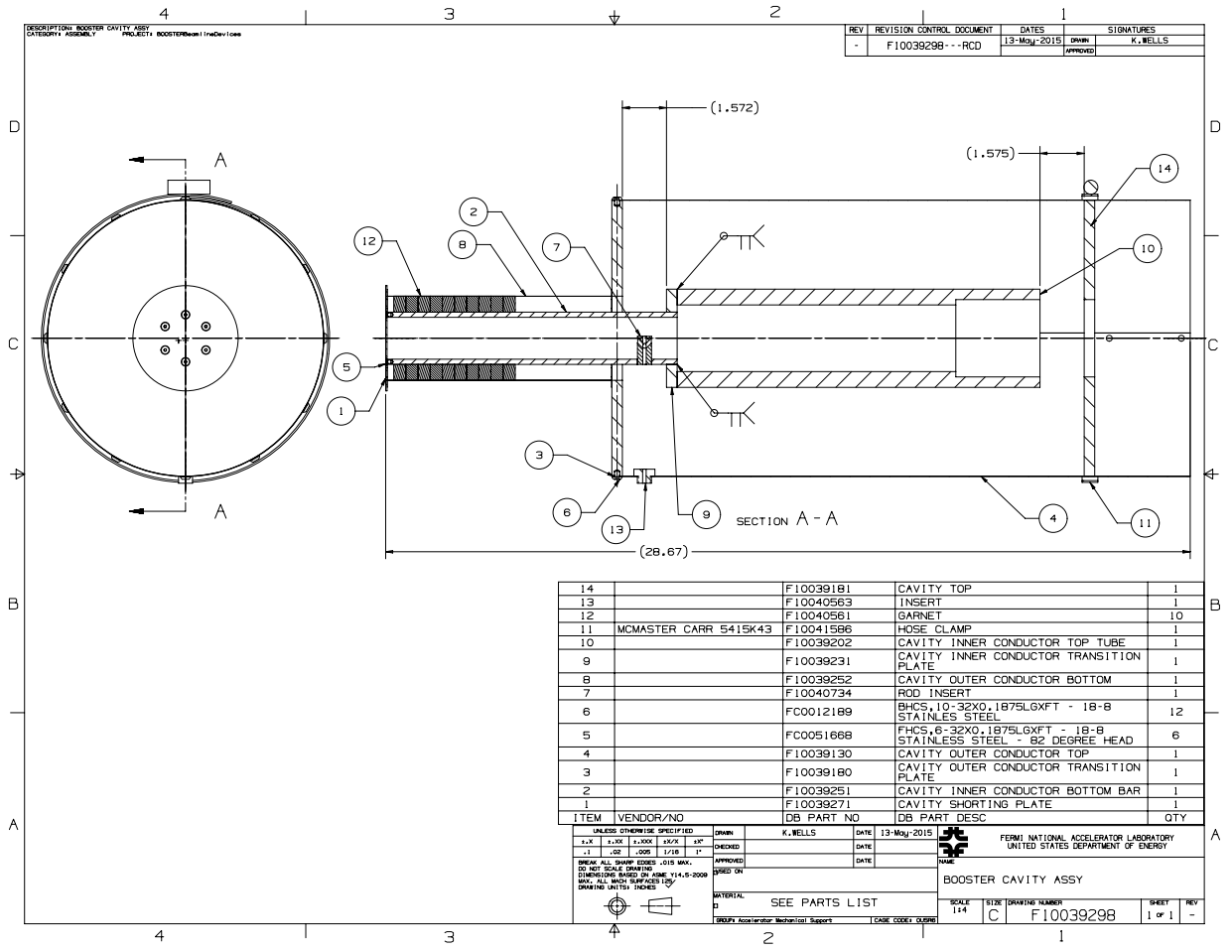

ITEM	VENDOR/NO	DB PART NO	DB PART DESC	QTY
14		F10039181	CAVITY TOP	1
13		F10040563	INSERT	1
12		F10040561	GARNET	10
11	MCMASTER CARR 5415K43	F10041586	HOSE CLAMP	1
10		F10039202	CAVITY INNER CONDUCTOR TOP TUBE	1
9		F10039231	CAVITY INNER CONDUCTOR TRANSITION PLATE	1
8		F10039252	CAVITY OUTER CONDUCTOR BOTTOM	1
7		F10040734	ROD INSERT	1
6		FC0012189	BHCS,10-32X0.1875LGXFT - 18-8 STAINLES STEEL	12
5		FC0051668	FHCS,6-32X0.1875LGXFT - 18-8 STAINLESS STEEL - 82 DEGREE HEAD	6
4		F10039130	CAVITY OUTER CONDUCTOR TOP	1
3		F10039180	CAVITY OUTER CONDUCTOR TRANSITION PLATE	1
2		F10039251	CAVITY INNER CONDUCTOR BOTTOM BAR	1
1		F10039271	CAVITY SHORTING PLATE	1

FIG. 3: The final blueprints for the model cavity. If this were a cavity designed for the Booster tunnel, the beam would enter from the left through a garnet section and see the accelerating gap at the right.

because we wanted to explore changes in this dimension within our error range for the construction. Modification three increased the outer diameter of the inner conductor in the garnet section from nominal 1.853 inches to 1.863 inches since the measured inner diameter of the manufactured garnets were larger than the initial specified value.

The quality factor and the shunt impedance of the ideal model cavity are shown as a function of resonant frequency in Fig. 4 with and without modifications. These plots show little change in the cavity due to these modifications. However, the range of the graphs in Fig. 4 are relatively large, so to quantify the effect of each modification, both the difference and percentage difference were calculated and plotted as a function of frequency and are shown in Fig. 5. Luckily, these small changes in the structure of the cavity have little effect

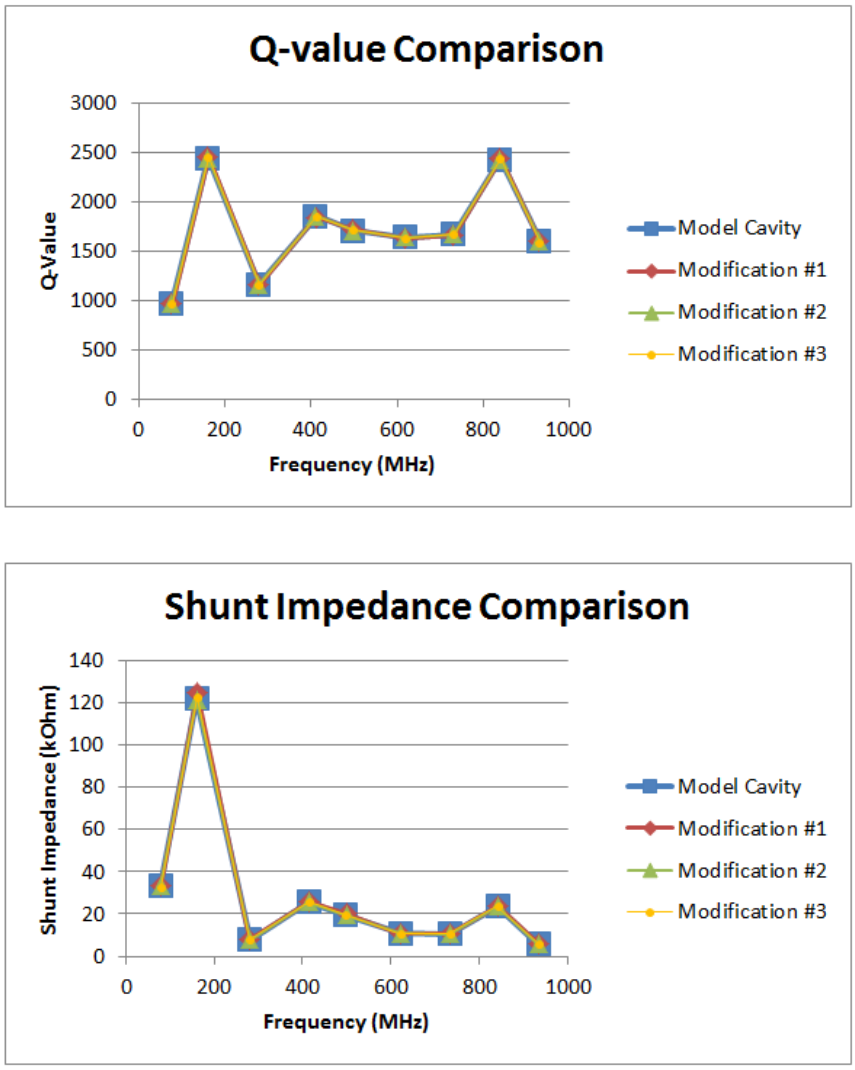

FIG. 4: The quality factor (labeled Q-value) and the shunt impedance of the model cavity as a function of frequency. The ideal model cavity is in blue with square markers and each of the individual modifications are shown with different colors and shapes. For this simulation, $\mu' = 3.5$, $\mu'' = 0.0024$, $\epsilon' = 13.86$ and $\epsilon'' = 0.0028$ where μ'' is calculated from Gennady Romanov's old μ-curve, see Section VI, Fig. 12.

on the quality factor and shunt impedance of the cavity.

Figure 4 shows that the trends in both the quality factor and shunt impedance are the same with each modification, and Fig. 6 shows that the greatest percent difference in quality factor is about 0.7% and in the shunt impedance is about 5%. One of the interesting qualities of these plots is that both the quality factor and shunt impedance peak at the first HOM.

Of the three changes, decreasing the inner diameter of the outer conductor in the air

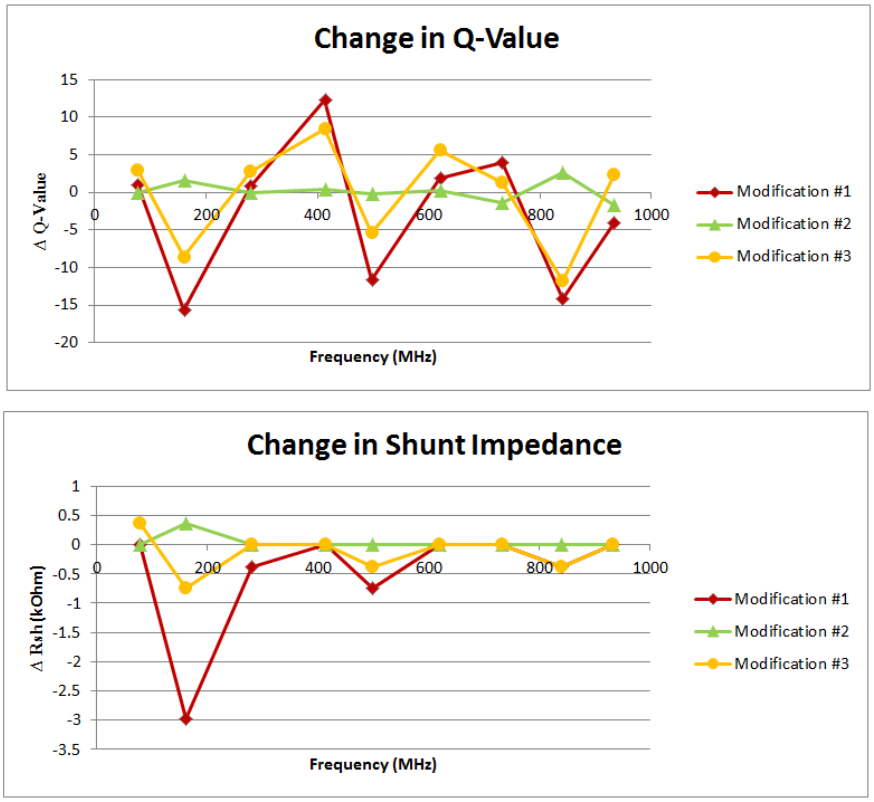

FIG. 5: The difference in quality factor and shunt impedance of the three modifications from the ideal model cavity. These values are plotted against the resonant frequencies of the ideal model cavity.

section (modification two) effected the cavity the least, which is a bit counterintuitive given it was the largest physical modification. The greatest effect on the cavity was produced by the smallest physical modification: changing the outer diameter of the inner conductor in the air section. Overall, these changes had a small effect on the properties of the cavity, and together change the quality factor by about 3% and the shunt impedance by about 15% [**?**].

It is important to note that the resonant frequencies of the model cavity change slightly with the modifications. Implementing all three modifications together raise the resonant frequencies by about 0.7% [**?**].

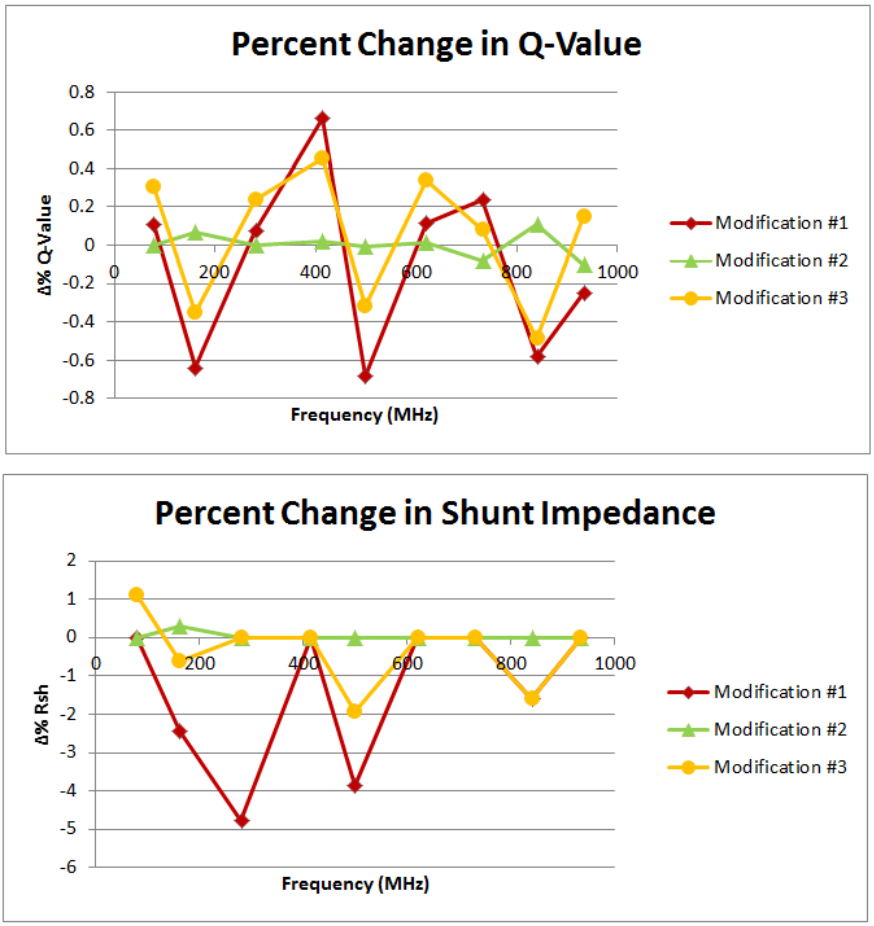

FIG. 6: The percent difference in quality factor and shunt impedance for the three modifications from the ideal model cavity. These values are plotted against the resonant frequencies of the ideal model cavity.

B. Change in Fundamental Frequency

In the Booster, the real cavity will be tuned to increasing resonant frequencies as the beam gains energy, ranging from approximately 76 MHz to 106 MHz. Having already investigated the characteristics of the cavity with fundamental frequency 76 MHz, next comes the study of the cavity at the highest resonant frequency, 106 MHz. To do this, a value of μ' was found and a complex permeability curve calculated by Gennady Romanov gave the values of μ'' [4].

Using the same Superfish code with modified permeability gives the quality factor and shunt impedance of the model cavity with the larger fundamental frequency. The resulting plots are shown in Fig. 7. In these plots, $\mu' = 3.5$ corresponds to the fundamental frequency

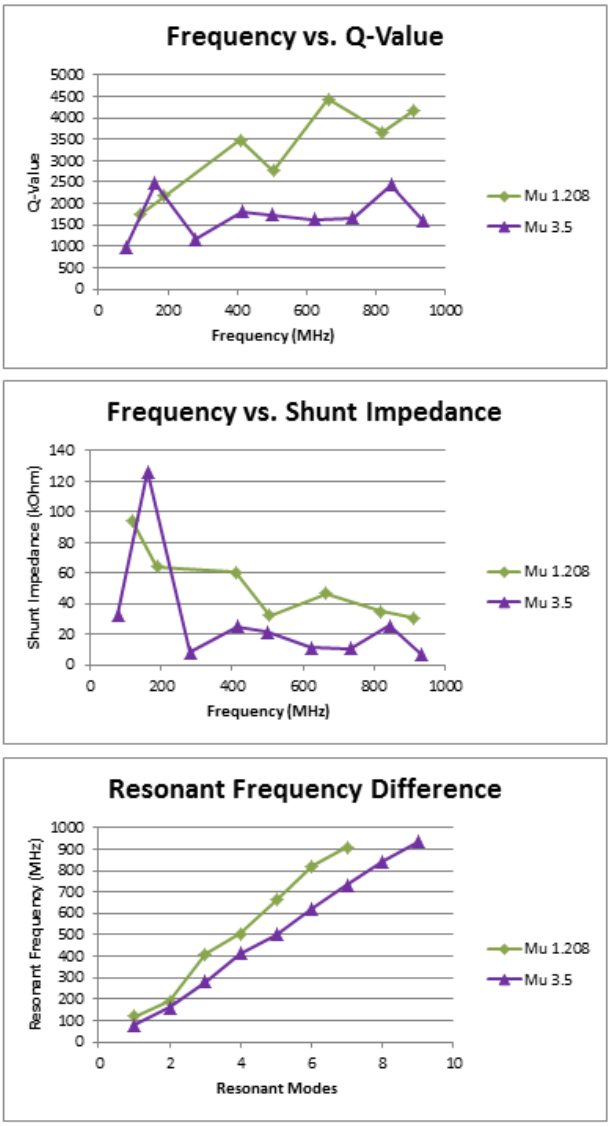

FIG. 7: The quality factor and shunt impedance of the model cavity with different μ' values. The bottom graph shows the frequency of each resonant mode. The large μ' shown by the purple triangles corresponds to fundamental frequency 76 MHz, while the small μ' shown by green diamonds corresponds to fundamental frequency 106 MHz. For this simulation, $\epsilon' = 13.86$, and $\epsilon'' = 0.0028$ where μ'' is calculated from the Gennady Romanov's old μ-curve.

76 MHz, and $\mu' = 1.208$ corresponds to fundamental frequency 106 MHz. Throughout this study the real permittivity is held constant at $\epsilon' = 13.86$, a value given by the manufacturer.

There is a significant difference in both the quality factor and shunt impedance for these two cases. The characteristic peak in quality factor and shunt impedance seen with the

large μ' is not present with the small μ'. Another important observation is that for high μ' the quality factor and shunt impedance are roughly constant over the range of frequencies (except for the peak at the first HOM), however small μ' shows an overall increase in the quality factor and decrease in the shunt impedance.

The last observation to make from Fig. 7 is that frequency spacing between HOMs is larger for low μ' than for high μ', decreasing the number of resonances in the same frequency range. Overall, the differences in complex permeability change the quality factor and shunt impedance significantly and will be studied further.

C. Change in Electric Loss Tangent

The last change that was made to the Superfish model cavity was a change in the complex permittivity. The loss tangent was calculated to be half of that originally estimated, and the lossy part of the permittivity of the garnet (ϵ'') was changed to be $\tan\delta_e = \times 10^{-4}$, half the original value. While holding $\epsilon' = 13.86$, ϵ'' is changed to 0.001386. Again, we wanted to see what kind of effect this had on the quality factor and shunt impedance of the model cavity, and again Poisson Superfish was used to find these values.

Figure 8 shows both quality factor and shunt impedance for the two choices of ϵ'' at high and low frequency, and it becomes clear that the lowered value of ϵ'' has only a small effect, raising the quality factor and shunt impedance less than 20%. This difference is most significant at the higher frequency. The change in frequency is not shown here because the difference was insignificant. To see this difference, reference [**?**].

IV. REAL CAVITY SIMULATIONS

A. Change in Fundamental Frequency

The second part of the Superfish simulations study is to look at the real Booster harmonic cavity design. In this section, the study is confined to the effects of tuning to different fundamental frequencies and changing the electric loss tangent value. The Superfish simulations were made using dimensions gathered from the model shown in Fig. 2.

The Superfish simulations were performed for the same μ' and μ'' values as the model cavity and the results are shown in Fig. 9. Here it is found that decreasing μ' increases

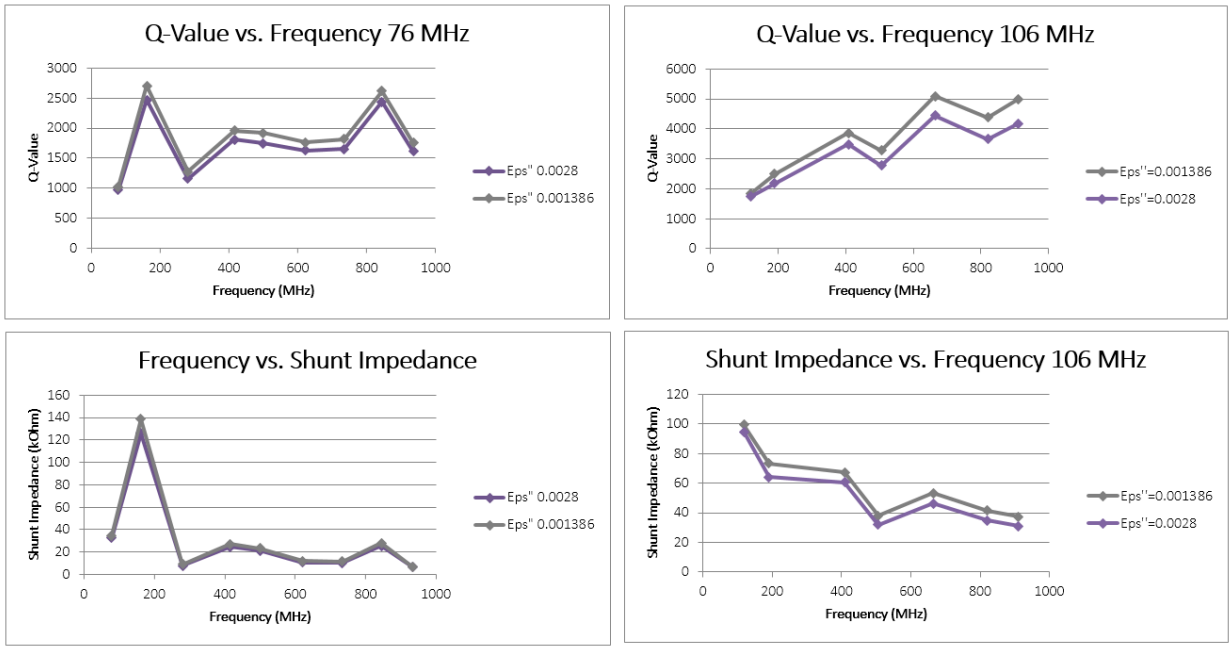

FIG. 8: The quality factor and shunt impedance of the model cavity with different values of ϵ'', the lossy component of complex permittivity. For these simulations, $\epsilon' = 13.86$, $\mu' = 3.5$, and $\mu'' = 0.0024$ where μ'' is calculated from Gennady Romanov's old μ-curve.

both the quality factor and the shunt impedance of the cavity. This is expected because the ferrite is moved further away from the lossy gyromagnetic resonance.

Analogous to the model cavity simulations shown in Fig. 7, we find that the quality factor and shunt impedance curves take on very different shapes with change in μ'. Similar to the model cavity, the real cavity with large μ' is approximately constant through the frequency range except for the spike at the first HOM. For the real cavity with small μ' we see a different trend. For the first four resonances the quality factor tends to increase and the shunt impedance tends to decrease. However, after the fourth resonance the two values alternate between high and low, producing spikes. This behavior differs even from the model cavity's steady increase or decrease through the entire frequency range.

Finally, the last plot of Fig. 9 shows the resonant frequencies of the cavity. Again, it can be seen that with the lower μ' value the frequency spacing between HOMs is larger producing fewer resonances in the same frequency range.

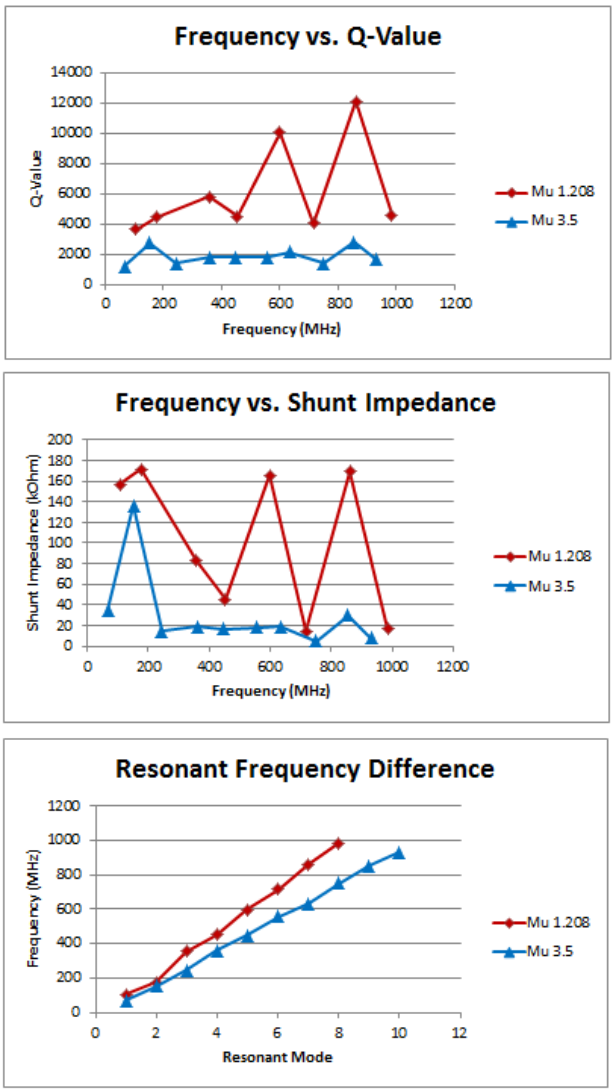

FIG. 9: The quality factor and shunt impedance of the real cavity with different μ' values. The bottom graph shows the frequency of each resonant mode. The large μ' shown by blue triangles corresponds to fundamental frequency 76 MHz, while the small μ' shown by red diamonds corresponds to fundamental frequency 106 MHz. For this simulation, $\epsilon' = 13.86$, and $\epsilon'' = 0.0028$ where μ'' is calculated from the Gennady Romanov's old μ-curve.

B. Change in Electric Loss Tangent

Now investigating the change in ϵ'', the lossy part of the permittivity, it is found that cutting the value in half changes little about the real cavity quality factor and shunt impedance, the comparison of which is shown in Fig. 10. In the same manner as the model cavity, cut-

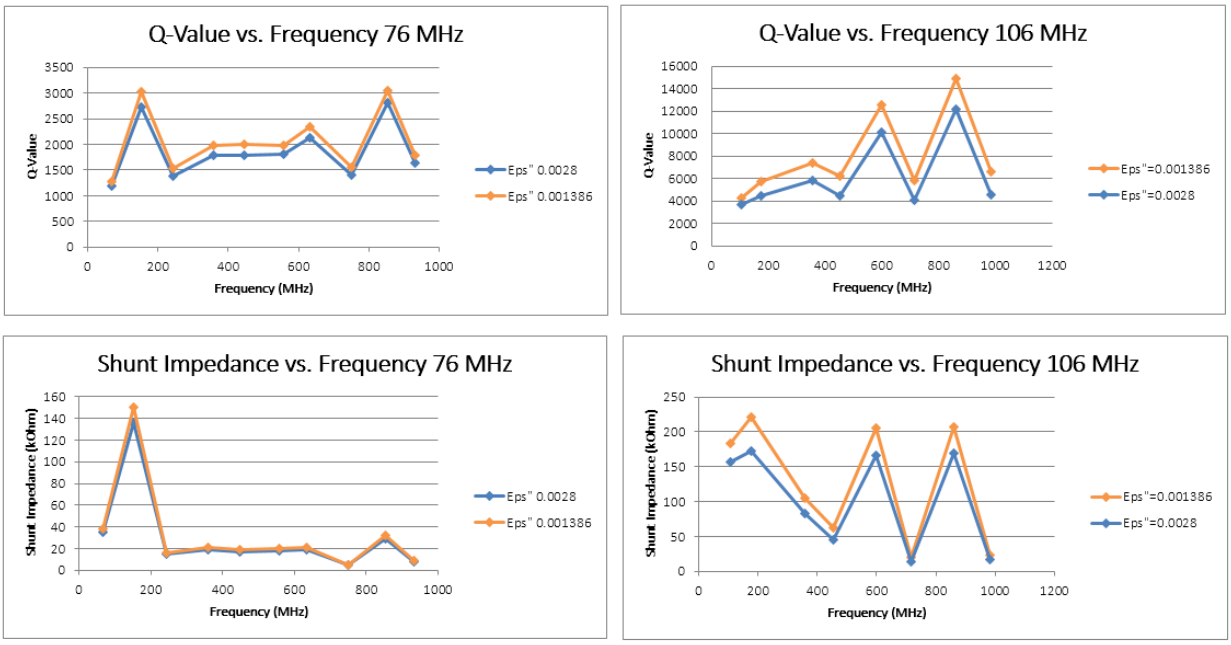

FIG. 10: The quality factor and shunt impedance of the real cavity with different values of ϵ'', the lossy component of complex permittivity. For these simulations, $\epsilon' = 13.86$, $\mu' = 3.5$, and $\mu'' = 0.0024$ where μ'' is calculated from Gennady Romanov's old μ-curve.

ting ϵ'' in half increases the qualtiy factor and shunt impedance by less than 20%. As in the model cavity, this change is greater at the higher frequency.

Since there is little difference in both the real and model cavity with the modified ϵ'' in the next steps of the project $\tan\delta_e = 1 \times 10^{-4}$, or in other words $\epsilon'' = 0.001386$, for the simulations unless otherwise stated.

V. MODEL CAVITY VERSUS REAL CAVITY

The culmination and final purpose of the previous studies is to compare the real and model cavity with each other. Previously, the study focussed on how the cavity reacted to change in μ''. Now we investigate one value of μ' at a time, comparing the real and model cavity together.

Starting first with the large μ', fundamental frequency 76 MHz, we turn our attention to Fig. 11, which shows both the model and real cavities to the left on the same plot. We find that, in general, the real cavity has a larger quality factor than the model. The two cavities follow the same trends through the first six resonance modes and both show a peak at the

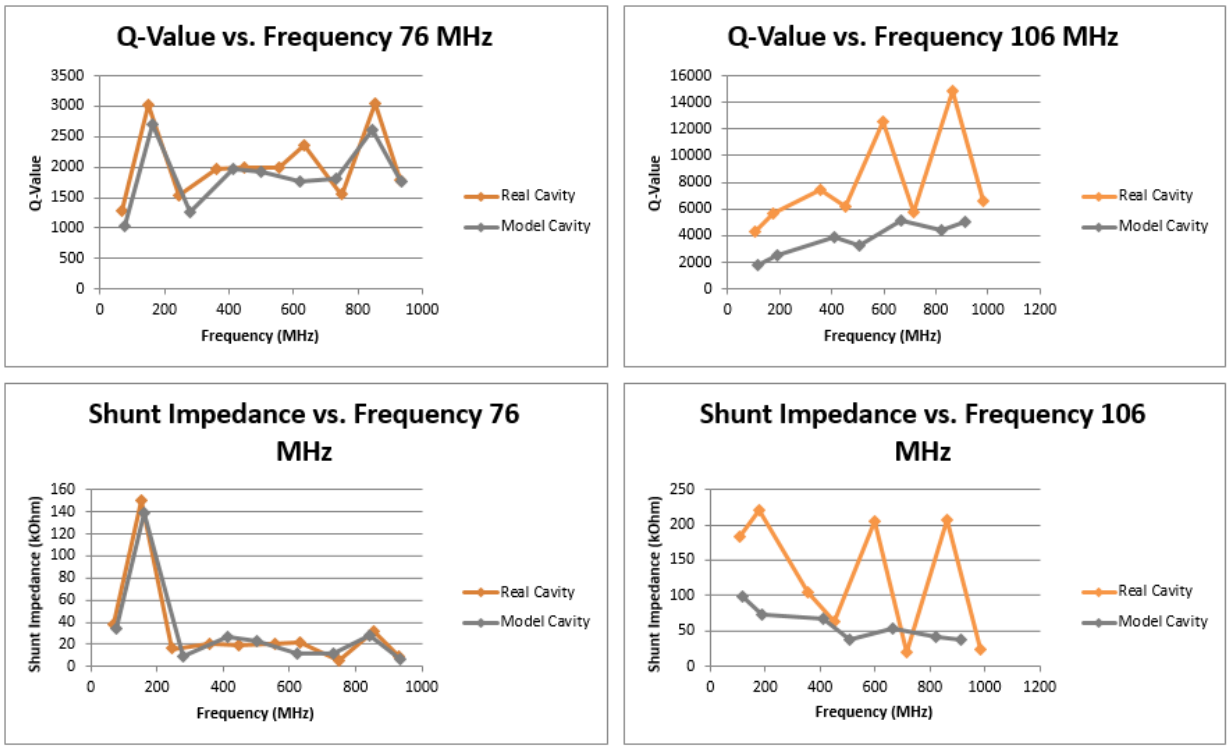

FIG. 11: Quality factor and shunt impedance of both the model and the real cavity plotted as a function of frequency. Here $\mu' = 3.5$ for the fundamental frequency 76 MHz and $\mu' = 1.208$ for the fundamental frequency 106 MHz. The last plot shows each resonant frequency. For these simulations, $\mu' = 3.5$, $\mu'' = 0.0024$, $\epsilon' = 13.86$, $\epsilon'' = 0.001386$.

first harmonic. The shunt impedance follows a similar trend. For the first three resonances the real cavity has a greater shunt impedance than the model, and overall the model and real cavities are very similar. Though not shown, again we find that the resonant frequency spacing of the model cavity is larger than the real cavity, leading to one less resonance in the same range. Overall, the model cavity seems to be a good approximation of the real cavity at this value of μ' at low fundamental frequency.

Now looking at the small μ' value, fundamental frequency 106 MHz, the comparison between real and model cavity is shown on the right of Fig. 11. Here the two cavities are significantly different. For the entire frequency range, the quality factor of the real cavity is significantly larger, in most modes at least doubled. The general trend is followed for the first four modes, but the values oscillate for higher modes. The shunt impedance of the real cavity is larger for most resonances, however is oscillates after the third HOM. While it

would be nice if the model cavity was a good approximation for the real cavity at 106 MHz, it is not as critical since we are most interested in the properties of the cavity at injection. Overall, it is good that the quality factor and shunt impedance of the real cavity is large so that the cavity has a large gap voltage for small power input.

At this larger frequency we find that the model does not approximate the cavity as well. As in the lower fundamental frequency, the real cavity has a higher quality factor and shunt impedance for the first few resonances. In this case, the difference between the model and real cavity is greater, especially after the fourth resonance.

Even though the quality factor and shunt impedance are quite different in this case, the resonant frequency plot looks very similar. Again, we find that the model cavity frequency changes more quickly and so has one less resonant mode in the same frequency range. Overall, though the model is a good approximation of the real cavity at the lower fundamental frequency, it is not a particularly good model at the higher fundamental frequency.

VI. COMPLEX PERMEABILITY CURVE OF FERRITE GARNET

As mentioned in the RF basics section, to fully characterize the cavity we must understand how both our tuning parameter and the loss change with bias field. In doing this, we parameterize μ'' so that we can write it as a function of μ'. In all the previous calculations, μ'' was found using the results from what is labeled as the thin plate experiment in Fig. 12.

More recently, Yuri Terechkine and Gennady Romanov improved upon this experiment, calculating both μ' and μ'' using a combination of iterative calculations and CST Microwave Studio. The experiment used a ferrite-filled quarter wave cavity inside a solenoid with a steel plug to increase the uniformity of the magnetic field through the ferrite. The results of this experiment are shown in green in Fig. 12 and called the steel plug experiment.

For the both the thin plate and the steel plug experiment shown in Fig. 12, the fits that express μ'' as a function of μ' are expressed as an exponential. While there is no fundamental reason to choose this type of fit, it produced the best R^2 value for the thin plate data and we used it for the steel plug experiment to be consistent.

The range of interest in Fig. 12 includes only between $\mu' = 1.2$ and $\mu' = 2.7$ because this is the range of permeability where the real cavity resonates at 76- 106 MHz. In this range

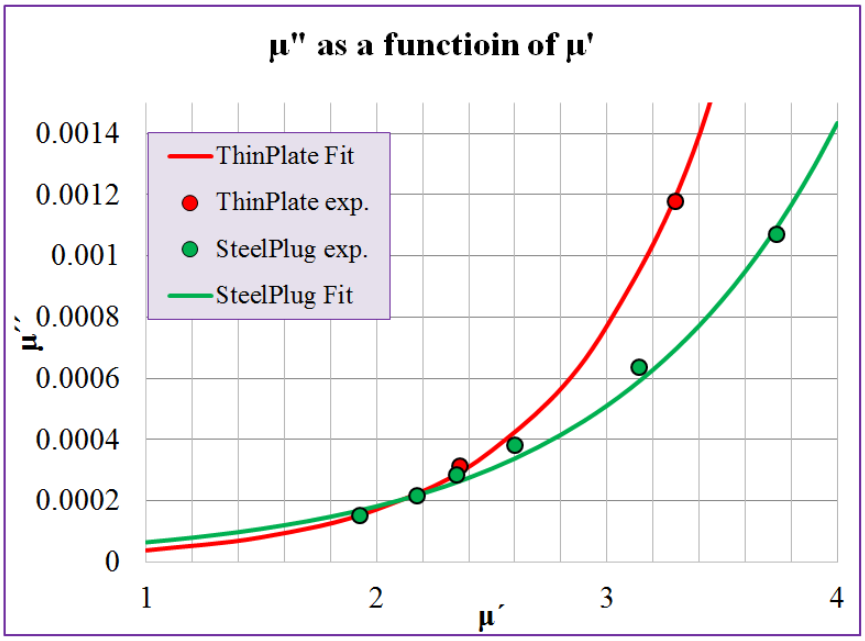

FIG. 12: Yuri Terechkine and Gennady Romanov's two calculations for μ' and μ''. The red data is the older calculation and is fit by the exponential curve $\mu'' = 8.572 \times 10^{-6}\ e^{1.5\mu'}$. The newer calculation is shown in green and is fit by an exponential curve $\mu'' = 2.316 \times 10^{-5}\ e^{1.0\mu'}$.

the two curves are very similar, the key difference being that at the low end of the range, the thin plate value is smaller and the high end of the range is larger. However this minor difference is well within our uncertainty range.

After these measurements and calculations were complete, we wanted to see how the μ-curve compared by algebraically calculating μ' and μ'', a simpler and less time-consuming process. We repeated the steel plug experiment technique but had a ferrite plug instead of a steel plug to increase the uniformity of the field in the ferrite. For this reason we called this the ferrite plug experiment.

The current in the solenoid was measured and with a network analyzer the corresponding resonant frequency and the loaded quality factor were determined. Correcting factors for the length of cables were determined for each frequency. These measurements were taken in the range 35-80 A solenoid current.

A. Calculating Q-Value

From these measurements, the unloaded Q-Value, and both real and imaginary parts of the permeability could be calculated. The S11 correction is a measure of how much power is reflected with respect to the forward power, and is defined as

$$S11(dB) = 10 \log \left(\frac{P_r}{P_f} \right), \tag{5}$$

where P_r is the reflected power and P_f is the forward power. The coupling factor, β, can also be defined using the ratio of reflected to forward power as

$$\beta = \frac{1 \pm \sqrt{P_r/P_f}}{1 \mp \sqrt{P_r/P_f}}. \tag{6}$$

Finally, the quality factor is expressed in terms of the coupling factor as

$$Q = Q_L(1 + 2\beta) \tag{7}$$

where Q_L is the loaded quality factor measured. The factor of two comes from the fact that there are two ports on the resonator.

B. Calculating μ'_{eff}

The next step is to calculate the effective μ'. Here the term effective is necessary because the garnet does not fill the entire volume of the cavity so there are two small gaps of air between the garnet and the copper cavity. Thus the effective permeability is corrected for these air sections. Starting from Eqn. 1 and the knowledge that the cavity is a quarter wave resonator we can make the replacement $\lambda = 4l$. Similarly we must understand that μ in Eqn. 1 is only the real part, so we can replace it with our new notation μ'_{eff} for the real effective permeability. Now solving for μ'_{eff} gives

$$\mu'_{eff} = \frac{1}{\epsilon_{eff}} \left[\frac{c}{4lf} \right]^2. \tag{8}$$

In Eqn. 8 all constants are known except for the effective permittivity, ϵ_{eff}, which can be found by calculating the capacitance of the cavity. In this case, we can divide the cavity into three sections: the inner air section that is bounded by the radius of the copper inner conductor (r_{icu}) and the inner radius of the garnet (r_{ig}), the garnet section, and the outer air section that is bounded by the outer radius of the garnet (r_{og}) and the radius of the copper outer conductor (r_{ocu}).

The general form of the capacitance per length of a coaxial line is

$$\frac{C}{l} = \frac{2\pi\epsilon\epsilon_0}{\ln(b/a)} \tag{9}$$

where b is the outer conductor and a is the inner conductor. In our case we have an effective permitivity that is associated with the total capacitance which can be found by adding the three capacitance regions in series. By doing this, the effective permitivity of the cavity is calculated to be

$$\epsilon_{eff} = \frac{ln(r_{ocu}/r_{icu})}{ln(r_{ocu}/r_{og}) + \frac{ln(r_{og}/r_{ig})}{\epsilon_{garnet}} + ln(r_{ig}/r_{icu})} = 10.015. \tag{10}$$

This value can then be used in Eqn. 8 to find μ'_{eff} as a function of frequency. In a similar manner, the permeability of the garnet only was calculated and found to be only about 2.5% different from the effective permeability.

C. Calculating μ''

Now that μ' is determined, we can calculate μ''. To do this we can start with the definition of quality factor, Eq. 4. Here the power dissipation comes from three sources: the copper, the magnetic loss and the electric loss. The total Q-value can then be expressed as

$$Q_{Tot} = \frac{\omega U}{P_{Cu} + P_{\mu''} + P_{\epsilon''}}, \tag{11}$$

where subscript Cu refers to the copper, subscript μ'' refers to magnetic loss an subscript ϵ'' refers to electric loss.

Inverting this expression we can rewrite the relationship as a sum of fractions

$$\frac{1}{Q_{Tot}} = \frac{P_{Cu}}{\omega U} + \frac{P_{\mu''}}{\omega U} + \frac{P_{\epsilon''}}{\omega U}. \tag{12}$$

By definition,

$$\frac{P_{Cu}}{\omega U} = \frac{1}{Q_{Cu}} \tag{13}$$

and ends up being the most useful part of the equation for finding the μ-curve. We also know from definition that

$$\frac{P_{\mu''}}{\omega U} = \frac{1}{Q_{\mu''}} = \tan\delta_B = \frac{\mu''}{\mu'}, \tag{14}$$

where $\tan\delta_B$ is the magnetic loss tangent, and finally we know from definition that

$$\frac{P_{\epsilon''}}{\omega U} = \frac{1}{Q_{\epsilon''}} = \tan\delta_E = \frac{\epsilon''}{\epsilon'}, \tag{15}$$

where $\tan\delta_E$ is the electric loss tangent and that we have measured this value to be 1×10^{-4}.

We can then rewrite Eqn. 12 as

$$\frac{1}{Q} = \frac{1}{Q_{Cu}} + \frac{1}{Q_{\mu''}} + \frac{1}{Q''_{\epsilon}}. \tag{16}$$

The quality factor of the copper can be found using [3] as a guide. We can simply change the inductance of the material. griffin uses $\mu = \mu_0$ because his cavity is under vacuum. However, since our cavity is filled with garnet material we can use $\mu = \mu'\mu_0$ instead. By making this small change in the inductance we can modify Griffin's final Q-value of the copper and solve Eqn. 16 for μ'' to find

TABLE I: Measured quantities Imon, frequency, loaded Q-value, and S11 as well as current, unloaded Q-value, μ_{eff}, and μ'' whose values were calculated in Excel. This includes all the data taken in the ferrite plug experiment.

Imon (V)	Current (A)	f_{meas} (MHz)	Q_L	S11 (dB)	β	$Q_{unloaded}$	μ_{eff}	μ''
1.604	80.359	118.838	2300	-0.1073	0.00618	2328	2.4658	0.0005214
1.397	69.991	113.587	2200	-0.0909	0.00523	2223	2.6990	0.0006465
1.200	60.124	107.605	2050	-0.0509	0.00293	2062	3.0075	0.0008519
0.999	50.057	100.107	1700	0	0	1700	3.4748	0.001379
0.901	45.148	95.745	1400	0	0	1400	3.7987	0.002009
0.799	40.039	90.571	1100	0	0	1100	4.2451	0.003101
0.701	35.131	84.277	500	0	0	500	4.9028	0.008970

$$\mu'' = \frac{\mu'}{Q} - 1 \times 10^{-4}\mu' - \frac{(1 + r_{ocu}/r_{icu})}{2r_{ocu}\sqrt{\pi f \mu_0 \sigma}\ln(r_{ocu}/r_{icu})}, \tag{17}$$

where σ is the conductivity of copper.

For easy reference, Table I includes the measured values from the network analyzer and the calculated values from Excel. The values in the table include all of the measured range, however the data fits are only in the μ' range of zero to four because it is our tuning region for the cavity.

D. Permeability Curve

Now that we have calculated μ' for each resonant frequency and parameterized μ'' in terms of μ' we we can study the curve μ'' versus μ', the complex permeability curve. The measurements were limited by the solenoid, so extrapolation is necessary to understand the relationship at low μ'. To be consistent with Gennady's curve fits, we fit the values in our range exponentially. This is shown in Fig. 13 with the steel plug curve fit by Gennady in Fig. 12.

To reiterate, both the steel plug and ferrite plug experiments were essentially the same. The difference comes from using an iterative calculation of multiple measurements of Q-

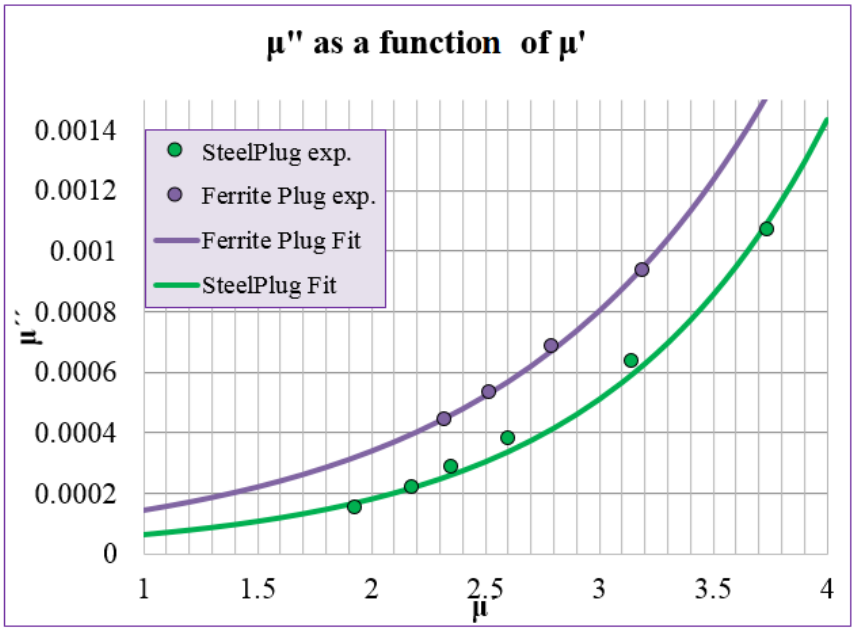

FIG. 13: The purple curve is the permeability curve calculated in the manner described in this paper, using the average Q-value. This curve is compared with the steel plug experiment which uses an iterative calculation to account for a non-uniform magnetic field in the ferrite. The exponential fit for the ferrite experiment curve is $\mu'' = 6.011 \times 10^{-5}\ e^{0.86\mu'}$.

value for each resonance for the steel plug experiment and using an average Q-value for an algebraic calculation in the ferrite plug experiment. The thin plate experiment was used to find μ'' in the previous sections but is a different experiment so is not included in the Fig. 13.

As expected, the two methods of calculating the complex permeability curve yield results with nearly the same curvature. The main difference between the two curves in Fig. 13 is the offset at the y-axis. The ferrite plug curve is then consistently larger than the steel plug values.

The algebraic calculation is insufficient to approximate the amount of cooling needed in the cavity to negate the losses, however further investigation is needed to determine if this ferrite plug experiment is good approximation when modeling the cavities. This item is addressed in the following section.

VII. THE EFFECT OF DIFFERENT μ'' VALUES ON THE CAVITIES

Using the three different complex permeability curves, we derive three values of μ'' for each value of μ'. Overall, we want to see what kind of effect this change has on each cavity. In short, can we use either the thin plate curve or the ferrite plug calculations to make a good approximation of the cavity's properties?

Using the method described before, I used Poisson Superfish to calculate the quality factor and the shunt impedance of both the real and model cavity at high and low fundamental frequency. In this case I used the newest model cavity with all of the modifications, as investigated above.

A. Real and Model Cavities Fundamental Frequency 76 MHz

To start the investigation, the three different values of μ'' for $\mu' = 2.7$ were calculated using the three different complex permeability curves. This value of μ' for 76 MHz is different than was previously used because this value makes the real cavity resonate at 76 MHz. The previously used value of $\mu' = 3.5$ made the model cavity resonate at 76 MHz. The Poisson Superfish simulation was again used to investigate the quality factor and shunt impedance of the cavities, changing only μ''. These results are shown in Fig. 14.

Again, since the calculated values in the steel plug experiment are the most precise, we are interested in comparing the other two curves with that.

First investigating the quality factor, both the thin plate curve and the ferrite plug curve have a lower value than the steel plug experiment for both the real and model cavity. The difference between the curves gets larger as the resonant frequency is increased, and for both cavities the ferrite plug curve is the most different.

Comparing the shunt impedance, the relative difference between the three curves appears to be constant as the frequency increases for both the real and model cavity. As with the quality factor, the steel plug curve gives the highest shunt impedance and the ferrite plug curve is the most different from it.

In order to evaluate the changes in the cavities more effectively, the thin plate and ferrite plug values were compared to the steel plug values and the percent differences are shown in Fig. 15.

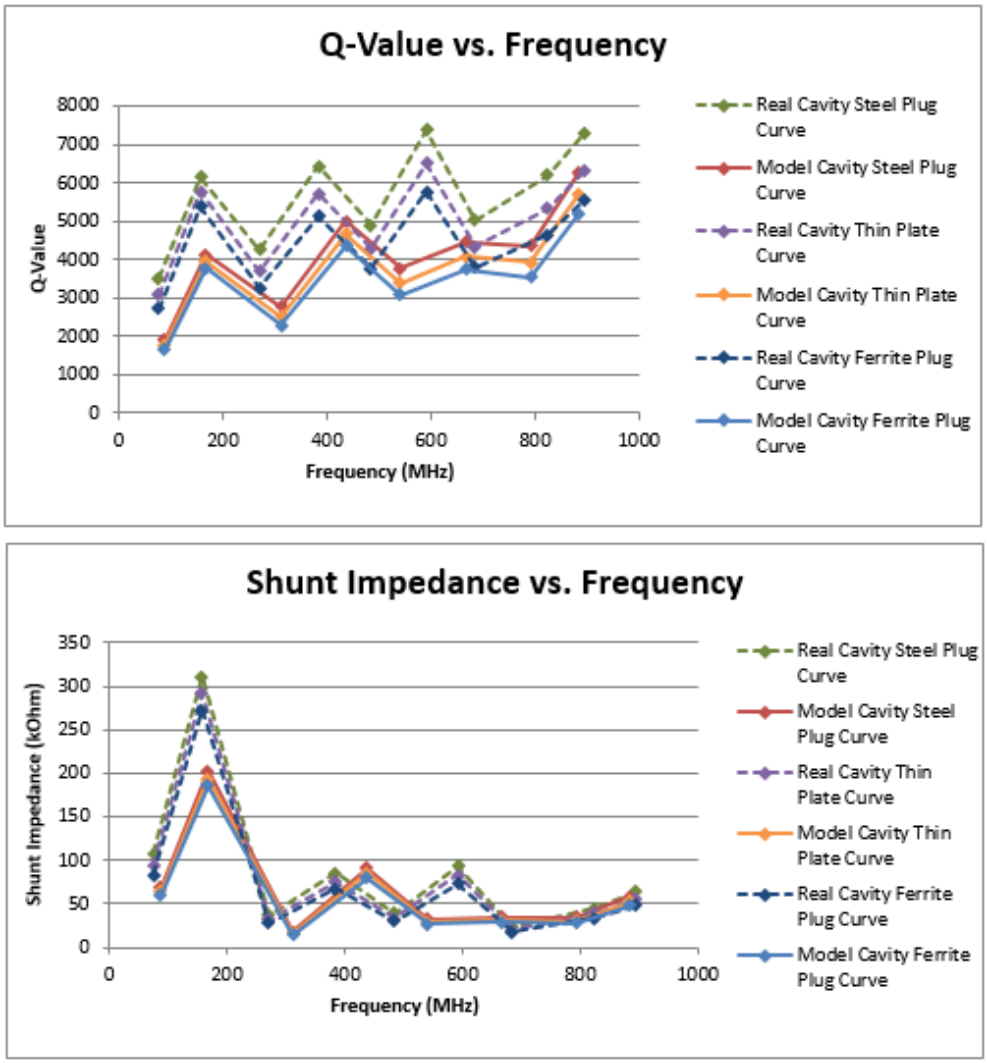

FIG. 14: The quality factor and shunt impedance as a function of frequency for three values of μ'' determined from the above experiments. Both the real (dashed lines) and model (solid lines) cavity values are shown. In this case the fundamental frequency is set to 76 MHz in the real cavity, with $\mu' = 2.7$. Other important parameters include $\epsilon' = 13.86$ and $\epsilon'' = 0.001386$.

This figure supports the observations above that the ferrite plug curve is the most different. In fact, it appears to have about twice the percent difference than the thin plate values. Another important observation is that the change in μ-curve has a greater impact on the real cavity. The greatest percent difference for the real cavity is around 25% while the greatest percent difference for the model cavity is around 19%.

Another interesting feature of Fig. 15 is that there is a drop in the percent difference at the first HOM. This is due to the spike in both the quality factor and the shunt impedance

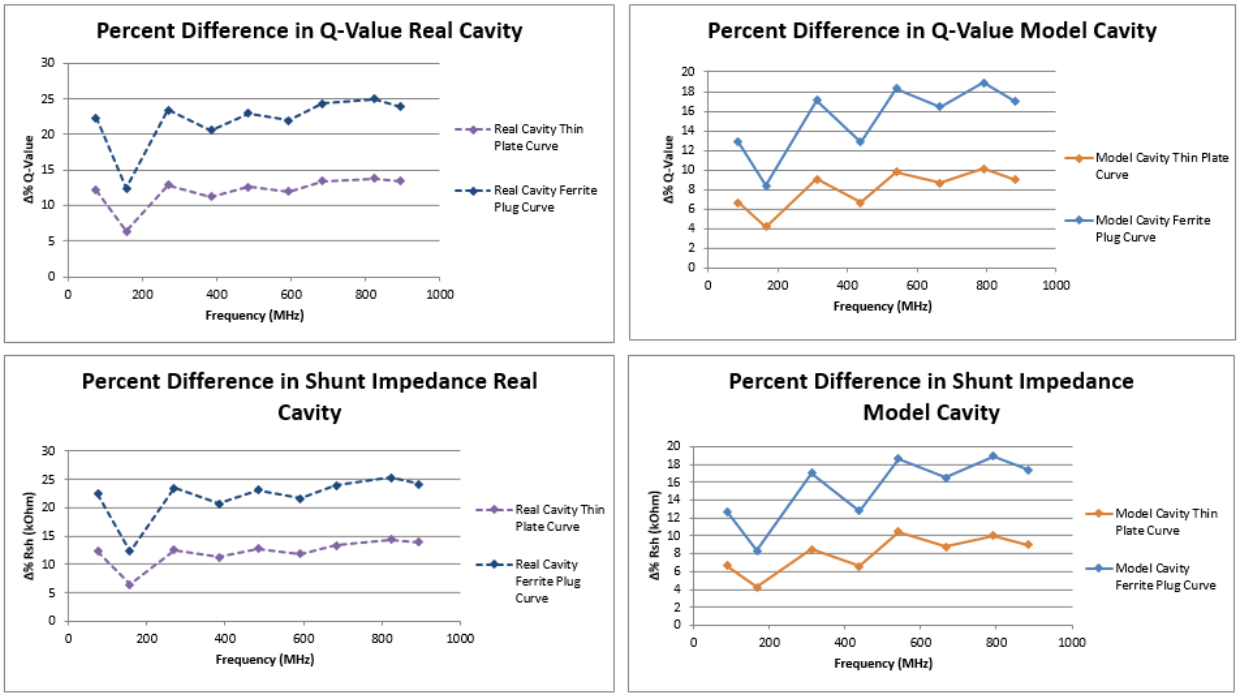

FIG. 15: Each plot shows the percent difference of the values from the steel plug curve values for fundamental frequency 76 MHz. The left column shows the real cavity and the right column the model cavity. Important parameters include $\mu' = 2.7$, $\epsilon' = 13.86$, and $\epsilon'' = 0.001386$.

at this frequency in both the real and model cavities. The spike is much more noticeable in the shunt impedance, but also occurs in the quality factor.

B. Real and Model Cavities Fundamental Frequency 106 MHz

Analogous to the study at 76 MHz fundamental frequency, Fig. 16 shows the quality factor and shunt impedance of both cavities using the three different μ-curves.

Looking at the quality factor we see that, unlike at high μ', the thin plate curve has a greater value than the steel plug curve over the entire frequency range for both real and model cavities. The ferrite plug curve has consistently lesser values than the steel plug for both real and model cavity, just as for high μ'.

For the shunt impedance we see a similar pattern. Again, the thin plate curve has greater values than the steel plug curve and the ferrite plug has less. This is again the case for both real and model cavities.

To investigate the differences further, we look turn to Fig. 17 which shows the percent

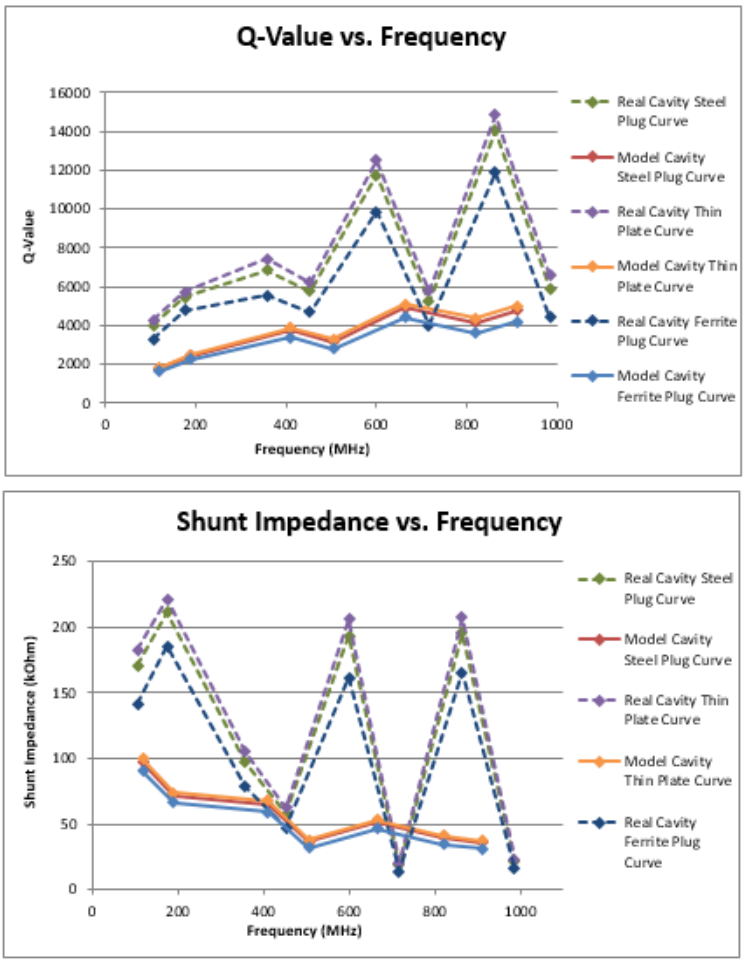

FIG. 16: The quality factor and shunt impedance as a function of frequency for three values of μ'' determined from the above experiments. Both the real (dashed lines) and model (solid lines) cavity values are shown. In this case the fundamental frequency is set to 106 MHz in the real cavity, with $\mu' = 1.208$. Other important parameters include $\epsilon' = 13.86$ and $\epsilon'' = 0.001386$.

difference of both thin plate and ferrite plug curves from the steel plug data. In this figure we see that indeed the thin plate values are greater than and the ferrite plug values are less than the steel plug data for both cavities. Again, we see that the ferrite plug values have about twice the percent difference of the thin plate values, although they are in the opposite direction now.

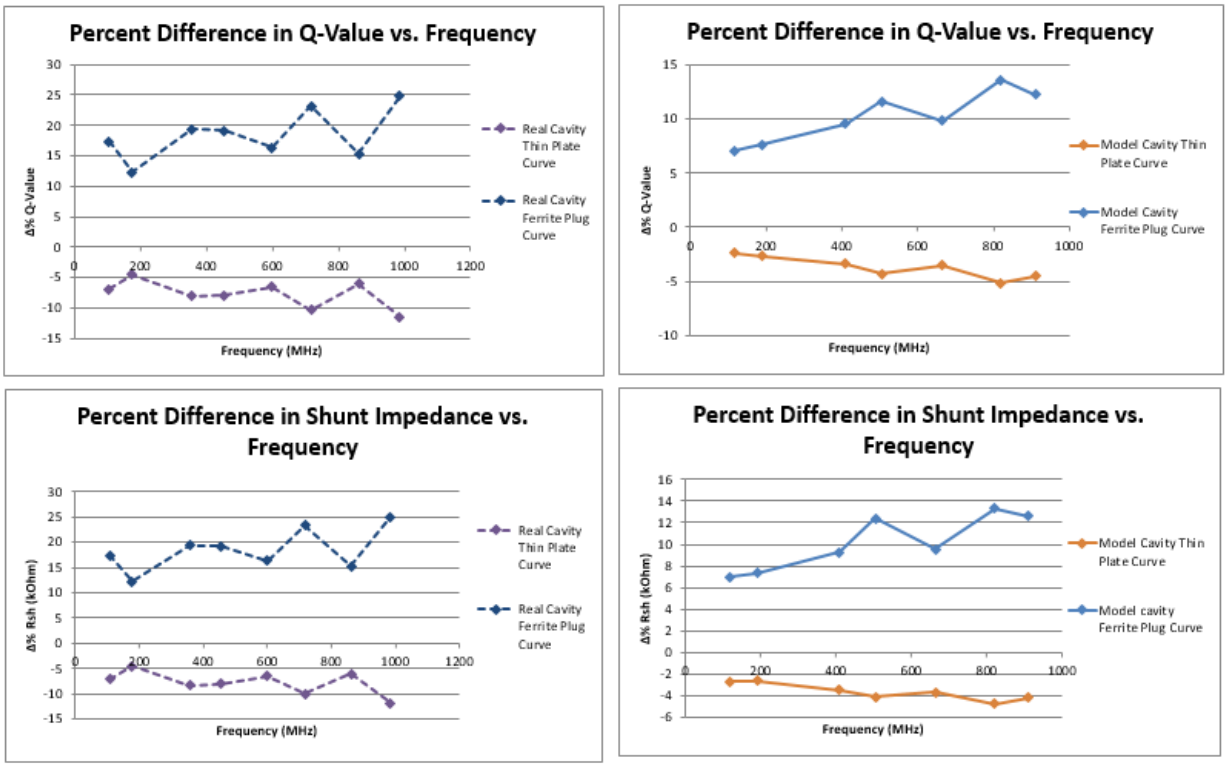

FIG. 17: Each plot shows the percent difference of the values from the steel plug curve values for fundamental frequency 106 MHz. The left column shows the real cavity and the right column the model cavity. Important parameters include $\mu' = 1.208$, $\epsilon' = 13.86$, and $\epsilon'' = 0.001386$.

VIII. POWER AMPLIFIER TEST STATION ELECTRONICS

In order to power the cavities, they are attached to power amplifiers. The purpose of these devices are to amplify the input signal and supply the cavity with RF. With the perpendicular biased cavity we can get more voltage gain by using the same power amplifier because there is less loss when compared to with the more often used parallel biased cavities. However, we must make sure that the power amplifier can supply the amount of power needed by the second harmonic cavity with the higher frequency RF.

The power amplifier is tested by attaching a quarter wave resonator, which acts like the cavity, and a load, which acts like the lossy ferrite to the device to create a test station. In order to test the power amplifier at this new resonant frequency (76 MHz), we need to build a new test station. The modifications are shown in Fig. 18 and include building a new resonator of a different shape, changing the position of the load, and replicating the

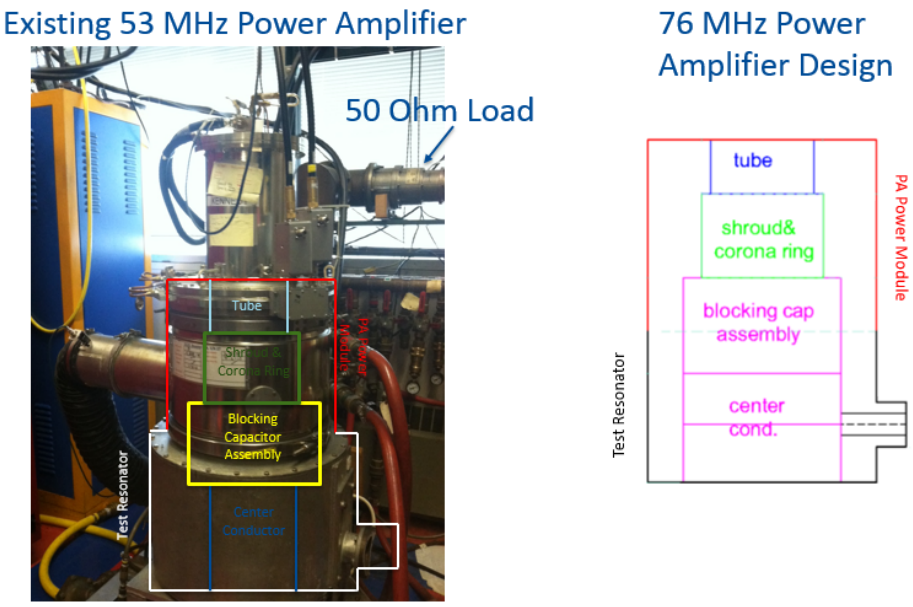

FIG. 18: A basics design for both the existing 53 MHz power amplifier test station superimposed on a picture of the station and the designs of the new 76 MHz power amplifier test station.

electronics needed to make the measurements.

The way that we test the output of the power amplifier is we measure the power dissipation in the load. This can be done by measuring the change in temperature of the cooling water between the incoming and outgoing flow. The change in temperature can easily be converted to power dissipation through the specific heat equation

$$\Delta Q = mC\Delta T, \tag{18}$$

where ΔT is the change in temperature, Q is the heat added to the system, m is the mass of the water, and C is the specific heat of the water. Using the rate of water flow in the cooling system, we can calculate the mass of water that travels through the lines over any given time, m/t. Also, we know that heat added, Q, is the amount of energy added to the water and that power is the rate of change of energy, dQ/dt. Choosing a set interval over which to solve, we are left with the equation

$$\frac{\Delta Q}{t} = \frac{m}{t}C\Delta T, \tag{19}$$

where we see that time dependence vanishes.

The specific heat of water is 4.186 J/g°C, so we can re-write the specific heat equation as

$$P = 4.186[flow]\Delta T, \tag{20}$$

where the power, P, is measured in kiloWatts. In our current set-up, we have an average power of 50 kW (200 kW for 25% on), and a flow rate of 14 gal/min which gives a temperature change of 13.57 °C.

The measurement of this change in temperature can be carried out using a resistance temperature detector (RTD). The idea of the RTD is that its resistance changes with temperature and this relationship is very well-known. We can then exploit this relationship to create electronics to measure the temperature of both the incoming and outgoing water channels.

The diagrams for these electronics, designed by Mitch Adamus are shown in Fig. 19. This diagram includes two circuits. First, located to the left we have the RTD circuit with converts the change in resistance to an output current. Second, located at the middle of the diagram we have a circuit that converts that input current into a temperature readout.

The first circuit uses two inputs, one through a 100 Ohm resistor and the other through the RTD, to measure the difference in resistance. This is converted in the chip to an output current signal.

In this case we have a offset to worry about because when the difference between the 100 Ohm resistor and the RTD is zero, we have an output current of 4 mA. This factor is accounted for in the second circuit in the initial series of resistors. This series is designed specifically to correct for the 4 mA current output. The variable resistor in the series is used to adjust the two output temperature readings during calibration.

The next step of the second circuit in Fig. 19 is a current to voltage op-amp. This configuration converts an input current to an output voltage. The second op-amp simply converts the negative voltage to a positive one, and we get the ideal input into the display chips.

We first built the current to voltage converter board, the second circuit. We then troubleshooted the circuit by supplying an input current to the board, mimicking the current output from the first board. We then measured the change in the temperature readouts over a range of current inputs, changing the variable resistor to different values so the displays would match. Figure 20 reports the final results of the this investigation, showing the difference between the calculated and measured temperature readouts as a function of

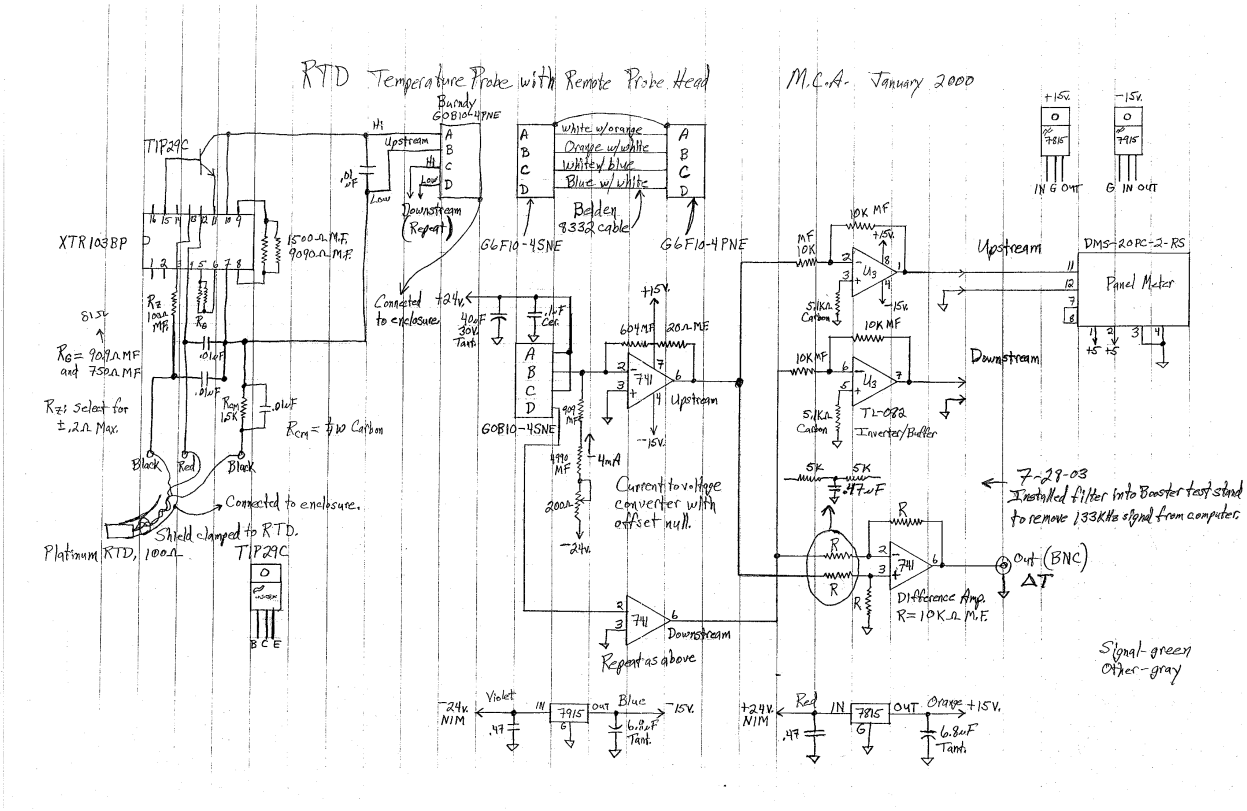

FIG. 19: A circuit diagram detailing the RTD electronics from the change in resistance to the temperature display readings. This circuit design and diagram are courtesy of Mitch Adamus.

temperature.

The most interesting feature about Fig. 20 is that the upstream and downstream displays do not have the same slope. Ideally, there a constant offset between the two that could be corrected for using the variable resistor. However, we have a slight difference in the offset at difference temperature ranges. Using Eqn. 20 we can find the error in the power measurements that would occur due to this offset. The largest difference between calculated and measured temperature is about 0.6 °C. Plugging this value in the ΔT of Eqn. 20 and solving for power with our current conditions listed above gives an error of 2.2 kW.

We then built the rest of the electronics shown in Fig. 19 and troubleshooted the device as a whole. To do this we taped the temperature probes together with copper tape to help insure that the probes were at the same temperature. We then put them in ice water and recorded the change in the temperature display readings over time, and repeated with boiling water.

When we found that there was a roughly constant offset between the two displays, we

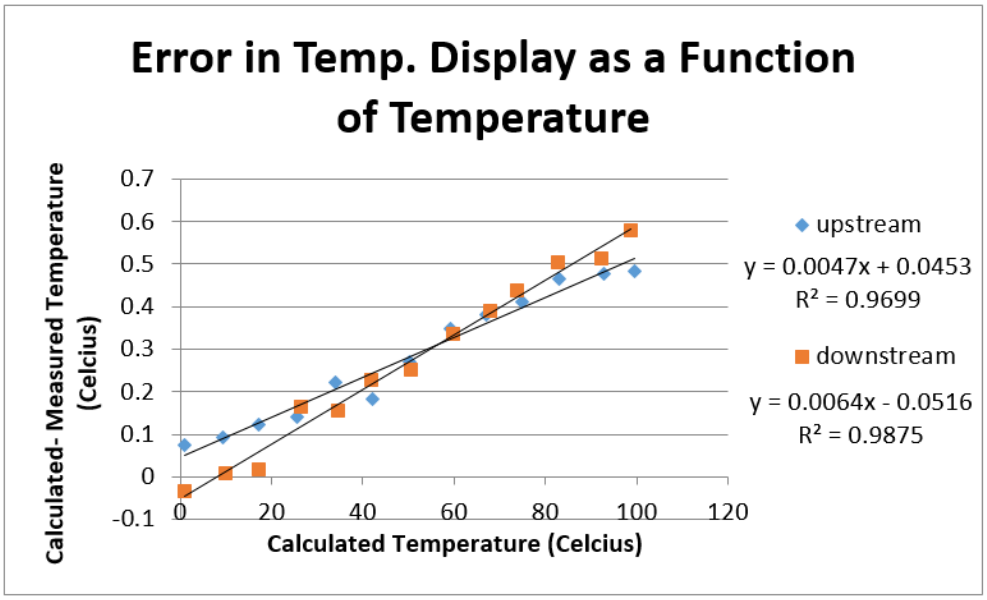

FIG. 20: A plot of the difference between the calculated and display temperature as a function of calculated temperature.

TABLE II: Final measured resistances of the resistor series used to calibrate the electronics, shown in Fig. 21.

	A-B	B-C
Upstream	5.99 kΩ	120.2 Ω
Downstream	6.06 kΩ	183.2 Ω

adjusted the variable resistor in the downstream side until the displays matched. Though we are unsure if the absolute temperature reading of the probes is accurate, we are most interested in the difference in temperature between the two probes. Currently, our difference in the temperature readings is up to 0.1 degrees Celsius when the two probes are at the same temperature. This results in an error for the power of ± 0.37 kW.

The final resistance values for the resistor series are shown in Table II for future reference. The labeled points referenced in the table are shown in Fig. 21.

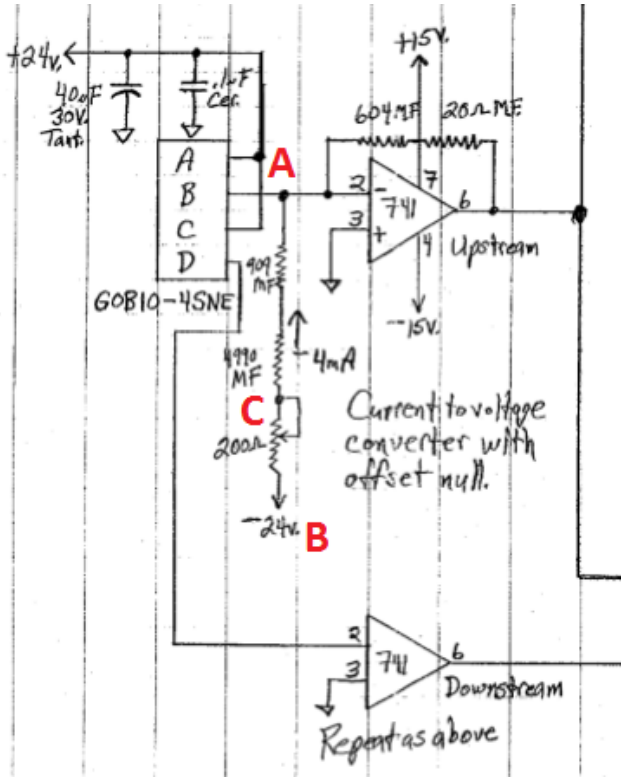

FIG. 21: A cut of the circuit diagram showing the labeled points on the resistor series used for adjustments.

IX. CONCLUSIONS

In conclusion, we have done a thorough comparison analysis of the real and model cavities using Poisson Superfish and have found that the structural changes have little impact on the model cavity behavior and that it compares well at the 76 MHz fundamental frequency, but diverge significantly at 106 MHz fundamental frequency.

We have also investigated the permeability of the ferrite in the magnetic field, and algebraically calculated both the tuning parameter and the lossy component assuming the losses are constant throughout the material. We found that there is a significant difference between these results and results originally found by Gennady Romanov, but that the algebraic method is a good enough approximation for the Superfish simulations.

Lastly, we have built and troubleshooted the electronics for the new power amplifier test

station using circuit diagrams from Mitch Adamus.

---

[1] *Poisson Superfish*, Los Alamos National Laboratory, Richard P. Feynman Center for Innovation Software, $http : //www.lanl.gov/projects/feynman - center/technologies/software/poisson - superfish.php$

[2] C. Y. Tan et al., *A Perpendicular Biased 2nd Harmonic Cavity for the Fermilab Booster*, in Proceedings of the 6th International Particle Accelerator Conference (IPAC15), Richmond, VA, May 2015.

[3] James E. Griffin, *Appendix. A Numerical Example of an RF Accelerating System*,

[4] Gennady Romanov, *On discrepancy between transmission model and 3D CST simulations*, for 2nd Harmonic Cavity Meeting, Fermilab, Batavia, IL, May 2015, $http : //beamdocs.fnal.gov/AD/DocDB/0048/004847/001/21May2015_2nd_Harm.pptx$.